

Perspective

# Optical Helicity and Optical Chirality in Free Space and in the Presence of Matter

Lisa V. Poulikakos <sup>1</sup>, Jennifer A. Dionne <sup>1</sup> and Aitzol García-Etxarri <sup>2,3,\*</sup>

<sup>1</sup> Department of Materials Science and Engineering, Stanford University, 496 Lomita Mall, Stanford, CA 94305, USA

<sup>2</sup> Donostia International Physics Center and Centro de Fisica de Materiales CSIC-UPV/EHU, Paseo Manuel de Lardizabal 4, 20018 Donostia-San Sebastian, Spain

<sup>3</sup> IKERBASQUE, Basque Foundation for Science, Maria Diaz de Haro 3, 48013 Bilbao, Spain

\* Correspondence: aitzolgarcia@dipc.org

Received: 17 July 2019; Accepted: 15 August 2019; Published: 3 September 2019



**Abstract:** The inherently weak nature of chiral light–matter interactions can be enhanced by orders of magnitude utilizing artificially-engineered nanophotonic structures. These structures enable high spatial concentration of electromagnetic fields with controlled helicity and chirality. However, the effective design and optimization of nanostructures requires defining physical observables which quantify the degree of electromagnetic helicity and chirality. In this perspective, we discuss optical helicity, optical chirality, and their related conservation laws, describing situations in which each provides the most meaningful physical information in free space and in the context of chiral light–matter interactions. First, an instructive comparison is drawn to the concepts of momentum, force, and energy in classical mechanics. In free space, optical helicity closely parallels momentum, whereas optical chirality parallels force. In the presence of macroscopic matter, the optical helicity finds its optimal physical application in the case of lossless, dual-symmetric media, while, in contrast, the optical chirality provides physically observable information in the presence of lossy, dispersive media. Finally, based on numerical simulations of a gold and silicon nanosphere, we discuss how metallic and dielectric nanostructures can generate chiral electromagnetic fields upon interaction with chiral light, offering guidelines for the rational design of nanostructure-enhanced electromagnetic chirality.

**Keywords:** optical chirality; optical helicity; nanophotonics; plasmonics; parity symmetry; time symmetry

## 1. Introduction

Chiral electromagnetic fields, exhibiting left- or right-handedness, have the ability to interact selectively with matter. In particular, the chiral molecular building blocks of biological matter, e.g., proteins and amino acids, exhibit distinct interactions with left- or right-handed light, thus enabling the visualization of the role of chirality in natural processes [1]. Additionally, the selectivity and sensitivity of chiral light–matter interactions has shown promise in a variety of technological applications. The development of pharmaceuticals faces the challenge of heterochirality, where an unbiased chemical reaction forms equal quantities of left- and right-handed products. Importantly, their biochemical interaction with patients can range from the desired pharmaceutical treatment to harmful side-effects by simply interchanging molecular chirality [2]. Thus, chiral light has been proposed as a non-invasive method to bias chemical reactions toward products of a single handedness [3–5] or to detect and separate molecules based on their chirality [6,7]. The chirality of light has additionally found potential in optical information storage and transfer [8,9], with the ability to increase capacity and selectivity.

The interaction between chiral electromagnetic plane waves, such as circularly polarized light (CPL), and matter is inherently limited in sensitivity due to their bounded spatial distribution. Rapidly-evolving research efforts in the field of chiral nanophotonics aim to address this challenge by the tailored design of metallic [10–28] and dielectric [29–38] nanostructures, arranged periodically in sub-wavelength metamaterials and metasurfaces, or in colloidal dispersions, achieving highly concentrated electromagnetic chirality in their evanescent field (see also review articles [25,39–42]). However, the rational design of enhanced electromagnetic chirality in the presence of matter requires the definition of physical observables by which to quantify the chirality of light. For this, the *optical helicity* and the *optical chirality* have been proposed, where each quantity has been altered from its free-space form to account for interactions with matter. While closely related, the optical helicity and the optical chirality differ in their physical meaning, and their application in the presence of matter is subtle yet distinct. This perspective performs a comprehensive comparison of each quantity and its physical significance in free space and in the presence of matter.

First, the optical helicity and optical chirality are introduced in the context of rotating vector fields and chiral symmetries, while the physical significance of each quantity in free space is discussed in analogy to the relationship between momentum and force in classical mechanics. Subsequently, the implications of optical helicity, optical chirality and their respective conservation laws upon interaction with microscopic and macroscopic matter are considered with a particular focus on the role of matter-induced losses. For this, an additional, physically-relevant comparison to energy and momentum conservation in classical mechanics is provided and the physical observables arising from the conservation law of optical chirality in lossy, dispersive media are discussed. Finally, we apply these observables to elucidate the physical mechanisms of chiral light–matter interactions in artificial nanostructures, where the distinct cases of metallic and dielectric nanoparticles are analyzed numerically. In particular, the chiral electromagnetic fields generated by gold and silicon nanospheres with 75 nm radius are considered, demonstrating in both cases that achiral, linearly polarized excitation does not yield a net electromagnetic chirality, while chiral excitation with left- and right-handed CPL results in mirror-symmetric optical chirality flux spectra.

## 2. Rotating and Handed Vector Fields

A rotating vector field is handed when its motion exhibits a non-zero component parallel to the rotational axis. This vector field property, found in a variety of natural phenomena [43,44], can be quantified by the *helicity*, a pseudoscalar resulting from projection of the angular momentum vector onto the linear momentum vector [45,46]. In fluid dynamics, the helicity is obtained from the projection of the fluid velocity  $\mathbf{v}$  onto its curl, also known as vorticity,  $\nabla \times \mathbf{v}$  [47]:

$$\mathcal{H}_{\text{fluid}} = \int \mathbf{v} \cdot (\nabla \times \mathbf{v}) d^3x. \quad (1)$$

In plasma physics, the magnetic helicity:

$$\mathcal{H}_{\text{magnetic}} = \int \mathbf{A} \cdot (\nabla \times \mathbf{A}) d^3x, \quad (2)$$

can be employed for the topological classification of a magnetic induction field  $\mathbf{B} = \nabla \times \mathbf{A}$ , with vector potential  $\mathbf{A}$  [48], where integration over all of space results in gauge invariance of Equation (2) [43,49]. In contrast to Equations (1) and (2), single-particle helicity has been quantified in quantized systems where, for instance, photon helicity amounts to  $\pm 1$  [43,46,50].

In classical electrodynamics, where Maxwell's equations describe the relationship between electric and magnetic fields, Equation (2) can be extended to define the *optical helicity* [43]:

$$\mathcal{H}_{\text{optical}} = \frac{1}{2} \int \left[ \sqrt{\frac{\epsilon_0}{\mu_0}} \mathbf{A} \cdot (\nabla \times \mathbf{A}) + \sqrt{\frac{\mu_0}{\epsilon_0}} \mathbf{C} \cdot (\nabla \times \mathbf{C}) \right] d^3x, \quad (3)$$

where  $\mathbf{C}$  is the electric pseudovector potential with  $\mathbf{E} = -\nabla \times \mathbf{C}$  for electric field  $\mathbf{E}$  in free space [43,49]. While the vector and pseudovector potentials  $\mathbf{A}$  and  $\mathbf{C}$  are gauge variant, upon integration over all of space in Equation (3), only their gauge-invariant transverse components are non-zero [43]. The integrand of Equation (3), termed *optical helicity density*, is the lowest-order term in an infinite set of conserved quantities [49,51], where higher orders are obtained by mapping the magnetic and electric vector potentials onto their curls:  $\mathbf{A} \rightarrow \nabla \times \mathbf{A}$  and  $\mathbf{C} \rightarrow \nabla \times \mathbf{C}$  [52,53]. The first-order transformation in this series yields the *optical chirality density*, a quantity identified as physically significant in the study of chiral light–matter interactions [54]. The corresponding volume-integrated *optical chirality* is written as [54,55]:

$$\Xi = \int \left[ \frac{\epsilon_0}{2} \mathbf{E} \cdot (\nabla \times \mathbf{E}) + \frac{1}{2\mu_0} \mathbf{B} \cdot (\nabla \times \mathbf{B}) \right] d^3x. \quad (4)$$

While both the optical helicity (Equation (3)) and optical chirality (Equation (4)) provide information on the handedness of electromagnetic fields, they are physically distinct quantities, exhibiting a proportionality in the case of monochromatic electromagnetic fields in free space [43].

### 3. Physical Significance of Optical Helicity and Optical Chirality in Free Space

Noether's theorem [56] states that a conserved quantity arises in the dynamic equations of any continuous symmetry of a nondissipative system. As demonstrated by Calkin in 1965 [57], the optical helicity density  $h$  (integrand of Equation (3)) is the conserved quantity related to *electromagnetic duality symmetry* in free space, where electromagnetic duality describes a transformation between electric and magnetic fields written as:  $\mathbf{E} \rightarrow \mathbf{E}_\theta = \mathbf{E} \cos\theta - \mathbf{H} \sin\theta$  and  $\mathbf{H} \rightarrow \mathbf{H}_\theta = \mathbf{E} \sin\theta + \mathbf{H} \cos\theta$  [50,57].

Concurrently in 1964, Lipkin utilized Maxwell's equations to identify a new conservation law, naming the conserved quantity *Lipkin's zilch* [55]. It was not until 2010 when the physical significance of Lipkin's zilch was identified by Tang and Cohen as the local density of electromagnetic chirality, now known as the optical chirality density  $\chi$  (integrand of Equation (4)).

The optical helicity density  $h$ , the optical chirality density  $\chi$  and their respective flux densities  $\Phi$  and  $\mathbf{F}$ , follow formally analogous continuity equations in free space, as indicated in Table 1. This congruence along with the ability of both the optical helicity and optical chirality to describe the handedness of electromagnetic fields opens the question on how to distinguish these quantities, as discussed below.

**Table 1.** Conservation laws of optical helicity (left column) and optical chirality (right column) in free space with optical helicity density  $h$ , optical helicity flux density  $\Phi$ , optical chirality density  $\chi$ , optical chirality flux density  $\mathbf{F}$ , electric vector potential  $\mathbf{C}$ , magnetic vector potential  $\mathbf{A}$ , electric field  $\mathbf{E}$ , and magnetic induction field  $\mathbf{B}$ .  $\epsilon_0$  and  $\mu_0$  represent the free-space electric permittivity and magnetic permeability.

Optical Helicity Conservation in Free Space	Optical Chirality Conservation in Free Space
$h = \frac{1}{2} \left[ \sqrt{\frac{\epsilon_0}{\mu_0}} \mathbf{A} \cdot (\nabla \times \mathbf{A}) + \sqrt{\frac{\mu_0}{\epsilon_0}} \mathbf{C} \cdot (\nabla \times \mathbf{C}) \right]$	$\chi = \frac{\epsilon_0}{2} \mathbf{E} \cdot (\nabla \times \mathbf{E}) + \frac{1}{2\mu_0} \mathbf{B} \cdot (\nabla \times \mathbf{B})$
$\Phi = \frac{1}{2} \left[ \sqrt{\frac{\epsilon_0}{\mu_0}} \mathbf{A} \times (\nabla \times \mathbf{C}) - \frac{1}{\epsilon_0} \mathbf{C} \times (\nabla \times \mathbf{A}) \right]$	$\mathbf{F} = \frac{1}{2} \left[ \mathbf{E} \times (\nabla \times \mathbf{B}) - \mathbf{B} \times (\nabla \times \mathbf{E}) \right]$
$\frac{\delta h}{\delta t} + \frac{1}{\mu_0} \nabla \cdot \Phi = 0$	$\frac{\delta \chi}{\delta t} + \frac{1}{\mu_0} \nabla \cdot \mathbf{F} = 0$

The physical significance of the optical helicity density has been described with the help of dimensional analysis, as it has units of angular momentum density ( $\frac{\text{N m s}}{\text{m}^3}$ ) [43,52,58]. Here, we extend this dimensional analysis to the optical chirality density  $\chi$  with units of force density ( $\frac{\text{N}}{\text{m}^3}$ ). Their respective units of angular momentum and force invite a qualitative comparison to the relationship between momentum and force in classical mechanics, illustrated in Table 2.

**Table 2. Top:** The relationship between force and momentum for linear and rotational motion in classical mechanics, for linear momentum  $\mathbf{p}$ , force  $\mathbf{F}$ , angular momentum  $\mathbf{L}$ , and torque  $\boldsymbol{\tau}$ . **Bottom:** The relationship between the optical helicity density  $h$  and the optical chirality density  $\chi$  in classical electrodynamics.

Physical Significance	Fundamental	$\rightarrow$	Observable
<b>Classical Mechanics</b>			
Linear Motion: $\frac{d\mathbf{p}}{dt} = \mathbf{F}$	Linear Momentum [N s]	$\frac{d}{dt} \rightarrow$	Force [N]
Rotational Motion: $\frac{d\mathbf{L}}{dt} = \boldsymbol{\tau}$	Angular Momentum [N m s]	$\frac{d}{dt} \rightarrow$	Torque [N m]
<b>Classical Electrodynamics</b>			
Handed Motion: $h \xrightarrow{\nabla \times} \chi$	Optical Helicity Density [ $\frac{\text{N m s}}{\text{m}^3}$ ]	$\xrightarrow{\nabla \times}$	Optical Chirality Density [ $\frac{\text{N}}{\text{m}^3}$ ]

For a closed system with time-invariant mass, Newton's second law states that the net force exerted on the system is equal to the time derivative of the linear momentum (first row in Table 2). Similarly, for rotational motion in classical mechanics, the angular momentum is obtained from the time derivative of the torque (second row in Table 2). Equivalent information can, therefore, be obtained from the conservation of momentum and the conservation of force. However, momentum conservation, from which force conservation can be derived, is more generally valid. In contrast, for practical applications, forces lend themselves more easily to measurement and observation [59,60].

Inspired by classical mechanics, we draw a similar comparison for optical helicity and optical chirality (third row in Table 2) [61,62]. While the vector potentials inherent to the optical helicity are not directly physically observable, the optical chirality depends only on uniquely defined and observable field quantities derived from Maxwell's equations. In contrast, the optical chirality is a higher order transformation of the optical helicity. Thus, while both the optical helicity density  $h$  and the optical chirality density  $\chi$  can provide information on the local handedness of an electromagnetic field in free space,  $h$  is the more fundamental quantity, while  $\chi$  is more suitable for experimental observation.

### Chiral Symmetries in Electromagnetism

After establishing the optical chirality density and flux as physically observable quantities which describe electromagnetic chirality, this section applies symmetry relations to illustrate how these quantities represent the chirality of electromagnetic fields [61]. A chiral system exhibits *parity odd* and *time even* symmetries [54,63]. For a function  $f(x, y, z)$  with spatial coordinates  $x$ ,  $y$ , and  $z$ , parity transformation occurs by inversion of the spatial coordinates through the origin. Specifically,  $f$  is parity odd when  $f(x, y, z) = -f(-x, -y, -z)$  [63,64]. In addition, a function  $f$  is time even when inversion of the temporal coordinate  $t$  results in  $f(t) = f(-t)$  [63,64]. Thus, chiral systems can take on two left- and right-handed mirror-symmetric forms. For chiral electromagnetic quantities  $\chi$  and  $\mathbf{F}$  (as defined in Table 1), the parity and time symmetries are noted in Table 3, resulting from the parity odd and time even symmetry of the electric ( $\mathbf{E}$ ) field and the parity even and time odd symmetry of the magnetic induction ( $\mathbf{B}$ ) field. To elucidate their physical origin, we now construct the symmetry relations of the  $\mathbf{E}$  and  $\mathbf{B}$  fields from source charges and currents.

**Table 3.** Parity and time symmetries of the optical chirality density  $\chi$  and the optical chirality flux density  $\mathbf{F}$ .

Physical Quantity	Tensor Rank	Parity Symmetry	Time Symmetry
Optical Chirality Density $\chi$	3	Odd (pseudoscalar)	Even
Optical Chirality Flux Density $\mathbf{F}$	1	Even (pseudovector)	Even

A static electric field is induced by interaction between positive and negative point charges (Figure 1a). For spatial coordinates  $(x, y, z)$ , an electric field vector  $\mathbf{E} = (E, 0, 0)$  is induced by a positive point charge at  $(-x, 0, 0)$  and a negative point charge at  $(+x, 0, 0)$ . Parity inversion directs the electric field vector along  $-x$ , whereupon the parity-odd electric field vector becomes  $\mathbf{E}_{\text{parity inversion}} = (-E, 0, 0)$ . The time-even symmetry of  $\mathbf{E}$  results from invariance of the polarity of the point charges upon time reversal.

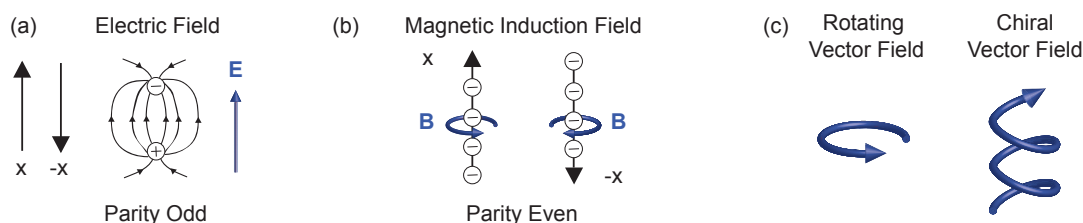


**Figure 1.** Illustration of parity symmetry for an electric field ( $\mathbf{E}$ ) arising between positive and negative point charges (a) and the magnetic induction field ( $\mathbf{B}$ ) arising from a steady state current (b). (c) Illustration of the distinction between a rotating vector field and a chiral vector field, where rotational motion has a component along the axis of rotation.

Figure 1b illustrates how a static magnetic induction field  $\mathbf{B}$  is induced by a temporally steady-state current. While a current along  $+x$  results in a clockwise rotation of  $\mathbf{B}$ , parity inversion, directing the current along  $-x$ , leads to anti-clockwise rotation of  $\mathbf{B}$ . Thus,  $\mathbf{B}$  is parity even due to the parity-odd symmetry of the curl operator [64]. Time inversion transforms the rotation of  $\mathbf{B}$  from clockwise to anti-clockwise as the current flows backwards temporally. With time invariance of the curl operator, the  $\mathbf{B}$  field is, therefore, time odd. Building on these fundamental examples, the parity and time symmetries of chiral electromagnetic quantities, as noted in Table 1, are now discussed.

Regarding *parity symmetry*, the optical chirality density  $\chi$  (Table 1) is a parity-odd pseudoscalar, attributed to the scalar product of a vector (the  $\mathbf{E}$  field or the curl of the  $\mathbf{B}$  field) and a pseudovector (the  $\mathbf{B}$  field or the curl of the  $\mathbf{E}$  field). In contrast, the optical chirality flux density  $\mathbf{F}$  (Table 1) is a parity-even pseudovector, its flux integral thus being parity odd. As shown in Figure 1c, rotating vector fields, e.g., the parity-even fields  $(\nabla \times \mathbf{E})$  or  $\mathbf{B}$ , do not exhibit the symmetries of a chiral quantity [65], as their signs remain invariant upon parity inversion. Thus, a parity-odd pseudoscalar is obtained from the product of these rotating fields with their related vector fields  $\mathbf{E}$  or  $(\nabla \times \mathbf{B})$ , respectively [61].

We now describe the *time symmetry* of a chiral electromagnetic system by comparison to a right-handed helical chiral object, the handedness of which is invariant upon forwards or backwards motion in time. Similarly, a chiral electromagnetic field exhibits rotational motion about its axis and the handedness of this motion remains unchanged under time reversal. This time-even property of chiral electromagnetic fields is seen in the optical chirality density  $\chi$  due to the projection of the  $\mathbf{E}$  or  $\mathbf{B}$  fields onto their respective curl [61].

#### 4. Physical Significance of Optical Helicity and Chirality upon Interaction with Matter

The free-space definitions of optical helicity and optical chirality (Table 1), require further consideration in systems where light interacts with matter. In general, the presence of matter breaks duality symmetry and the conservation of optical helicity, as predicted by Noether's theorem [56], is no longer valid. In contrast, the conservation law of optical chirality in the presence of matter requires no such restrictions in the electric and magnetic fields or the material properties. Indeed, matter has been identified as a source or sink of optical chirality [54,66,67]. While both conservation laws of optical helicity and optical chirality have been modified from their free-space form to account for interactions with matter [44,50,68–71], this section discusses the distinction in their physical relevance and applicability.

To better differentiate optical helicity and optical chirality conservation in the presence of matter, we again draw a qualitative comparison between classical mechanics and classical electrodynamics. Figure 2a illustrates the elastic (left panel) and inelastic (right panel) collision of two moving objects with masses  $m_1, m_2$  and velocities  $\mathbf{v}_1, \mathbf{v}_2$ , respectively. For elastic collision (left), both the linear momentum  $\mathbf{p} = m\mathbf{v}$  and the mechanical energy, specifically the kinetic energy, of the system are conserved at times  $t_1$  before the collision and  $t_2$  after the collision. In contrast, while the inelastic collision (right) conserves the linear momentum  $\mathbf{p}$  of the system, the mechanical energy is no longer conserved as a portion is converted into other forms of energy (predominantly heat) [59]. Importantly, the comparison of elastic and inelastic collisions in Figure 2a reveals how the dissipation of kinetic energy in the inelastic collision is only represented by energy conservation and is not accounted for by momentum conservation. Momentum and energy conservation can thus provide equivalent information in the lossless case of an elastic collision. However, their utility differs in the dissipative case of an inelastic collision.

While physically distinct, the example of elastic and inelastic collisions in classical mechanics is instructive for the qualitative understanding of optical helicity and optical chirality conservation in matter. The presence of microscopic sources, in the form of point charges and currents, breaks duality symmetry due to the existence of electric charges and the absence of magnetic charges in matter [64]. Under constraint of the divergence-free transverse component of the current density, the conservation law of optical helicity has been reformulated to account for the presence of microscopic sources [44,70]. However, as this definition depends on vector potentials, where non-locality is circumvented by restricting the fields to their transverse components, the resulting source term is not directly physically observable. In contrast, the conservation law of optical chirality in the presence of microscopic material sources has been defined as a direct consequence of Maxwell's equations, resulting in a source term composed solely of physical, observable quantities [54]:

$$\frac{\delta\chi}{\delta t} + \frac{1}{\mu_0} \nabla \cdot \mathbf{F} = -\frac{1}{2} (\mathbf{j}_0 \cdot \nabla \times \mathbf{E} + \mathbf{E} \cdot \nabla \times \mathbf{j}_0), \quad (5)$$

where the source term arising from microscopic matter is shown on the right-hand side of Equation (5) and  $\mathbf{j}_0$  is the primary current density.

Figure 2b illustrates the physical relevance of optical helicity and optical chirality conservation in the presence of macroscopic matter, in systems free of primary sources. The left panel of Figure 2b shows chiral light interacting with a piecewise homogeneous, isotropic medium with constant  $\epsilon_i/\mu_i$  over all material domains  $i$  [50]. Under these conditions, duality symmetry holds and both optical helicity and optical chirality are conserved [50]. Duality symmetry can also be induced in cylindrically symmetric dielectric objects and collections of objects under specific excitation conditions [72–74], also leading to helicity conservation. The conservation of optical helicity has proven instrumental in the analysis of the conversion of CPL into light with orbital angular momentum (OAM) [75–78]; it has also enabled generation of enhanced optical mirages from dual nanospheres [79,80] and an improved, elegant understanding of the interaction of vortex beams with well-defined helicity and macroscopic matter [81].

The right panel of Figure 2b represents a lossy, dispersive medium interacting with chiral light. In this case, the presence of matter breaks duality symmetry in the studied system and the optical helicity is no longer conserved in its physically observable form. In contrast, the conservation law of optical chirality can be extended from its free-space form (Table 1) to account for the presence of lossy, dispersive media, as outlined below in Section 4.1 [66,67]. Note that duality symmetry can also be broken in non-dispersive media where  $\epsilon \neq \mu$ .

The definition of optical helicity in the presence of material losses faces a set of challenges: For divergence-free displacement fields, the electric vector potential  $\mathbf{C}$ , inherent to the optical helicity, is written as  $\mathbf{E} = -\nabla \times \mathbf{C}$  [49]. Gauss' law in the presence of sources and currents,  $\nabla \cdot \mathbf{D} = \rho_0$  [64], elucidates two cases for which this condition is met (i) systems free of primary sources ( $\rho_0 = 0$ )

and (ii) lossless media. Systems obeying (i) and (ii) have been rigorously studied in previous work [50,68,71,82]—note that the model presented in [71] can be applied to systems with negligible material losses, such as perfect metals.

For applications in nanophotonics, we focus on chiral light–matter interactions in artificial nanostructures composed of linear, homogeneous, isotropic media, where material losses can play a significant role in the generation of chiral electromagnetic fields [66,67,83]. We consider time-harmonic electromagnetic fields with notation  $\mathbf{E}(\mathbf{r}, t) = \text{Re}[\mathcal{E}(\mathbf{r})e^{-i\omega t}]$  for the electric field, where  $\mathcal{E}(\mathbf{r})$  is the complex electric field amplitude of the electric field at spatial coordinate  $\mathbf{r}$ . For short-hand notation, we write complex field amplitudes as  $\mathcal{E}(\mathbf{r}) = \mathcal{E}$ . In linear media, the complex electric permittivity  $\epsilon = \epsilon_0(\epsilon' + i\epsilon'')$  has its imaginary part of the relative permittivity  $\epsilon'' = \sigma(\mathbf{r}, \omega)/(\epsilon_0\omega)$ , where  $\sigma$  is the conductivity and  $\mathcal{J}_{\text{cond}} = \sigma(\mathbf{r}, \omega)\mathcal{E}(\mathbf{r})$  is the complex amplitude of the conduction current density. We then reformulate Gauss' law as [61,64]:

$$\nabla \cdot \mathbf{D} = \nabla \cdot (\epsilon_0\epsilon'\mathcal{E}) + \frac{i}{\omega} \underbrace{\nabla \cdot (\sigma(\mathbf{r}, \omega)\mathcal{E})}_{\nabla \cdot \mathcal{J}_{\text{cond}} = i\omega\rho_{\text{cond}}(\mathbf{r})} = \rho_0(\mathbf{r}), \quad (6)$$

with angular frequency  $\omega$ . Equation (6) demonstrates that the electric displacement fields are not divergence free in lossy media. Specifically, the underbrace in Equation (6) shows time-harmonic charge continuity, from which Gauss' law can be reformulated as:  $\nabla \cdot (\epsilon_0\epsilon'\mathcal{E}) = \rho_0(\mathbf{r}) + \rho_{\text{cond}}(\mathbf{r})$ .

Thus, revisiting the case of an elastic and inelastic collision in classical mechanics (Figure 2), we draw a qualitative comparison to the physical relevance of optical helicity and optical chirality in the presence of matter. From Noether's theorem, the conservation of linear momentum in a lossless system arises from translational invariance [50,56] and, as Figure 2 demonstrates, the conservation of linear momentum captures the translational motion of a mechanical collision. Similarly, the conservation of optical helicity, with units of angular momentum, finds its physically relevant application in the description of chiral symmetries of propagating electromagnetic fields in systems where electromagnetic duality symmetry holds. In contrast, just as energy conservation captures the conversion of kinetic energy to heat in the case of an inelastic collision, optical chirality conservation is the suitable conservation law to describe the physical mechanism of optical chirality dissipation in the presence of lossy, dispersive media.

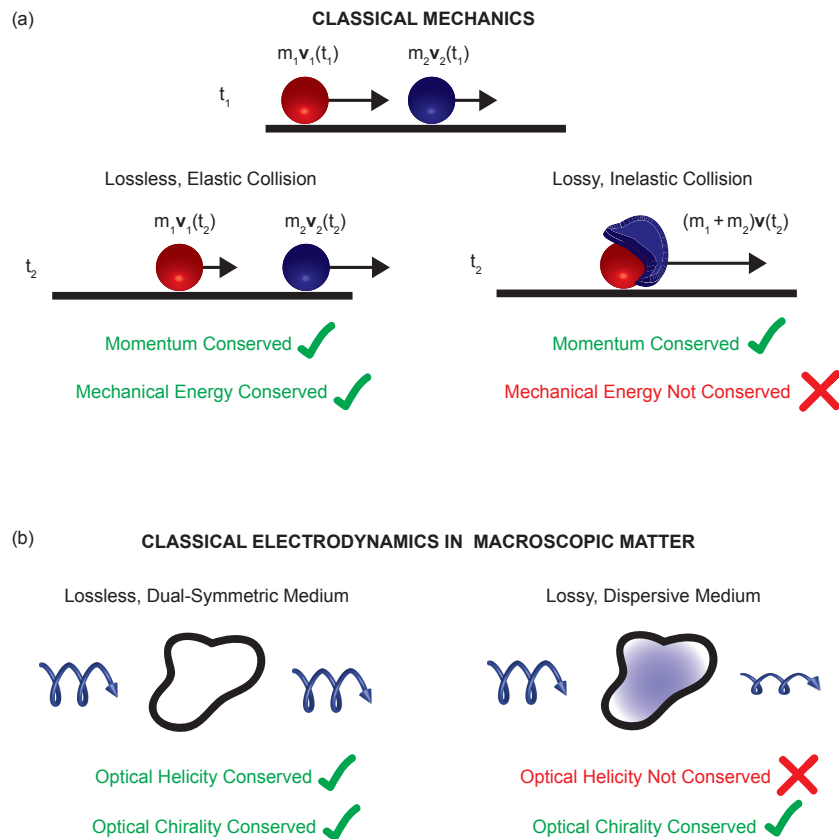


**Figure 2.** (a) Illustration of an elastic (**left**) and inelastic (**right**) collision of two objects with masses  $m_1$ ,  $m_2$ , moving at velocities  $\mathbf{v}_1$ ,  $\mathbf{v}_2$  at times  $t_1$ , before the collision (**top**) and  $t_2$ , after the collision (**bottom**), respectively. While the total linear momentum of the system  $\mathbf{p} = m\mathbf{v}$  is conserved for the elastic (**left**) and inelastic collision (**right**), the mechanical (kinetic) energy is not conserved for the inelastic collision due to energy dissipation. (b) Illustration of the interaction between chiral light and macroscopic matter for a lossless, dual-symmetric medium (**left**) and a lossy, dispersive medium (**right**). While both optical helicity and optical chirality conservation hold for the lossless, dual-symmetric case (**left**), the presence of a lossy, dispersive medium (**right**) breaks duality symmetry and helicity conservation no longer holds in its physically observable form. In contrast, the conservation law of optical chirality can be formulated to account for dissipative effects in the presence of lossy, dispersive media.

#### 4.1. Observables Derived from Chiral Electromagnetism

In systems free of primary sources for time-harmonic fields, the conservation law of optical chirality (Equation (5)) in linear, dispersive media with losses is written as [66]:

$$-2\omega \int_V \text{Im}(\chi_e - \chi_m) d^3x + \int_V \text{Re}(\nabla \cdot \mathcal{F}) d^3x = 0. \quad (7)$$

The first term in Equation (7) represents optical chirality dissipation:

$$\begin{aligned} \text{Im}(\chi_e - \chi_m) = & \quad (8) \\ & \frac{1}{8} [-\nabla \epsilon' \cdot \text{Im}(\mathcal{E} \times \mathcal{E}^*) - \nabla \mu' \cdot \text{Im}(\mathcal{H} \times \mathcal{H}^*)] \\ & + \frac{1}{4} \omega (\epsilon' \mu'' + \epsilon'' \mu') \text{Im}(\mathcal{E}^* \cdot \mathcal{H}), \end{aligned}$$

where  $\mathcal{E}$  and  $\mathcal{H}$  are complex field amplitudes of the electric and magnetic induction fields, with  $\epsilon = \epsilon' + i\epsilon''$  as the complex electric permittivity and  $\mu = \mu' + i\mu''$  as the complex magnetic permeability.

Equation (8) is composed of two physically distinct terms, where the first represents optical chirality dissipation arising from material anisotropy, expressed by the gradient of  $\epsilon'$  and  $\mu'$ , and the second describes optical chirality dissipation due to material loss, expressed by the imaginary parts of the material functions  $\epsilon''$  and  $\mu''$  [66,84]. The second term in Equation (7) represents the volume-integrated optical chirality flux, with density  $\mathcal{F}$  defined as:

$$\mathcal{F} = \frac{1}{4}[\mathcal{E} \times (\nabla \times \mathcal{H}^*) - \mathcal{H}^* \times (\nabla \times \mathcal{E})]. \quad (9)$$

In the far field, where electromagnetic fields are well-approximated as plane waves,  $\mathcal{F}$  can be represented by a weighted superposition of the optical chirality flux density arising from left- ( $\mathcal{F}_{LCPL}$ ) and right-handed ( $\mathcal{F}_{RCPL}$ ) circularly polarized plane waves, yielding a total far-field (FF) optical chirality flux  $\mathcal{F}_{FF} = |l|^2 \mathcal{F}_{LCPL} + |r|^2 \mathcal{F}_{RCPL}$ . The weighting factors for left- and right-handed CPL are represented by constants  $l$  and  $r$ , respectively. From this,  $\mathcal{F}_{FF}$  is directly proportional to the third Stokes parameter  $S_3$ , describing the degree of circular polarization, as [66,85]:

$$\mathcal{F}_{FF} = \frac{\omega}{c}(|l|^2 \mathcal{S}_{LCPL} - |r|^2 \mathcal{S}_{RCPL}) \propto S_3, \quad (10)$$

where  $c$  is the speed of light and  $\mathcal{S} = \mathcal{E} \times \mathcal{H}^*$  is the complex amplitude of the Poynting vector [64]. The optical chirality flux generated by lossy, dispersive media has been experimentally observed in the far field for periodic arrays of two-dimensionally chiral metallic nanoantennas [83] and colloidal dispersions of three-dimensionally chiral metallic nanopyramids at the single-particle level [86]. These experimental results demonstrated how the optical chirality flux is a physically relevant far-field observable, with the ability to provide information on chiral light-matter interactions in the near and far field.

In addition to the physically observable description of optical chirality dissipation and flux, derived from the conservation law of optical chirality (Equation (7)), the optical chirality density  $\chi$  (Table 1) has the ability to locally quantify the chirality of electromagnetic fields which can be strongly enhanced upon interaction with matter. The free-space optical chirality density (Table 1) of time-averaged, time-harmonic fields is written as:

$$\bar{\chi} = -\frac{\omega}{2c^2} \text{Im}(\mathcal{E}^* \cdot \mathcal{H}) = -\frac{\omega}{2c^2} |\mathcal{E}| |\mathcal{H}| \cos(\beta_{i\mathcal{E},\mathcal{H}}), \quad (11)$$

where  $\mathcal{E}$  and  $\mathcal{H}$  are the complex electric field and magnetic field amplitudes,  $\beta_{i\mathcal{E},\mathcal{H}}$  is the angle between the product  $i\mathcal{E}$  and the  $\mathcal{H}$  field, and the overbar in  $\bar{\chi}$  denotes the time average. Tang and Cohen identified Equation (11) within the excitation rate equation for chiral molecules [54]. This finding revealed the possibility to increase chiral selectivity of molecular excitation by orders of magnitude, when chiral molecules interact with electromagnetic fields of enhanced  $\bar{\chi}$  [6]. Subsequently, the rapidly-developing research area of chiral nanophotonics, summarized in a series of review articles [25,40–42], devoted itself to constructing solutions to Maxwell's equations for which  $\bar{\chi}$  exceeds its corresponding value for CPL, where  $\bar{\chi}/|\bar{\chi}_{CPL}|$  was termed *optical chirality enhancement* by Schäferling et al. [87].

A single electromagnetic plane wave reaches its maximum value of  $\bar{\chi}$  at the circular polarization state, resulting in  $|\bar{\chi}|/|\bar{\chi}_{CPL}| = 1$  [83]. However, the scale discrepancy between chiral molecules and the wavelength of CPL results in inherently weak selectivity [54]. Optical chirality enhancement beyond unity coincides with the concentration of electromagnetic energy ( $w = w_e + w_m$ ), as  $\bar{\chi}$  is bounded by  $c|\bar{\chi}|/(\omega w) \leq 1$  for speed of light  $c$  and angular frequency  $\omega$  [88,89].

In free space, theoretical studies have predicted  $|\bar{\chi}|/|\bar{\chi}_{CPL}| > 1$  for the diffraction-limited focusing of a circularly polarized Gaussian beam or the appropriate superposition of two Gaussian beams with radial and azimuthal polarization [90,91]. To better match molecular dimensions, evanescent waves can achieve a theoretically-unlimited spatial concentration of electromagnetic fields at material interfaces [92], enabling optical chirality enhancement beyond the diffraction limit [83]. In particular,

artificial nanostructures, with dimensions comparable to the wavelength of light, show great promise for the rational design of concentrated chiral electromagnetic fields.

We now provide a physical interpretation on how the optical chirality density  $\chi$  and optical chirality flux density  $\mathcal{F}$  of electromagnetic fields (Table 1) can be enhanced upon interaction with matter. A qualitative comparison can be made to vortex flow in fluid dynamics [61]. From Equation (1), the helicity density of a fluid vortex is written as  $h_{\text{fluid}} = \mathbf{v} \cdot (\nabla \times \mathbf{v})$  for fluid velocity  $\mathbf{v}$  and vorticity  $\boldsymbol{\omega} = \nabla \times \mathbf{v}$  [47]. Further, the flux of the solenoidal vorticity  $\boldsymbol{\omega}$  is conserved,  $\nabla \cdot \boldsymbol{\omega} = 0$ , indicating that an equal number of vortices with clockwise or counterclockwise rotation crosses the boundary of a closed system [47].

The formal analogy between the  $\mathbf{v}$  field of  $h_{\text{fluid}}$  and the electric and magnetic fields of  $\chi$  allows for the interpretation of  $\chi$  as the wrapping density of electric and magnetic field lines around their rotation axis [54]. With increasing wrapping density along this axis,  $\chi$  will increase in value. Further, while they differ in form, the vorticity flux  $\nabla \cdot \boldsymbol{\omega} = 0$  can support the interpretation of the optical chirality flux  $\nabla \cdot \mathcal{F}$ . In particular,  $\nabla \cdot \mathcal{F} \neq 0$  when the boundary of a studied system is traversed by an excess of one handedness of chiral electromagnetic field lines.

In contrast to fluidics, the interplay between electric and magnetic fields gives rise to additional complexity in electromagnetic chirality. In particular, Maxwell's equations dictate that a magnetic field can be induced by the rotation of an electric field and vice versa [64]. Further, while solid interfaces can act as sources of fluid vorticity, affecting fluid flow on boundary layers [93], the conservation law of optical chirality (Equation (7)) elucidates how material charges and currents can act as sources or sinks of chiral electromagnetic fields. In particular, both material loss and anisotropy (Equation (8)) can result in the dissipation and generation of electromagnetic chirality [54,66,67,70,83].

## 5. Chiral Light–Matter Interactions in Artificial Nanostructures

The effective design and optimization of artificial nanostructures with respect to their chiral optical fields requires insight into the mechanism of their interaction with chiral light. This section discusses the ability of metallic and dielectric nanostructures to generate chiral electromagnetic fields and elucidates the physical mechanisms present in each case. Figure 3 shows numerical simulations of the optical chirality flux generated by gold (part a) and silicon (part b) nanospheres of 75 nm radius (COMSOL Multiphysics 5.3a, gold material functions from Johnson and Christy [94] and silicon material functions from Aspnes and Studna [95]). In both systems, linearly polarized plane-wave excitation (LP, black) does not generate an optical chirality flux. In contrast, excitation with left- (LCP, red) and right-handed (RCP, blue) circularly polarized plane waves results in mirror-symmetric optical chirality flux spectra. Thus, in an achiral system, such as the studied nanospheres, inversion of the sign of the excitation light source inverts the sign of the optical chirality flux generated by the nanostructure.

The conservation law of optical chirality (Equation (7)), which sets equal the physical mechanisms of optical chirality dissipation and optical chirality flux can explain the generation of chiral optical fields in Figure 3. In particular, a non-zero optical chirality dissipation arises from the interaction between the achiral nanospheres and the chiral excitation source, leading to the generation of an optical chirality flux. In contrast, prior work has shown that nanostructures with a chiral geometry interacting with achiral, linearly polarized light have the ability to dissipate optical chirality, thus generating an optical chirality flux [66,83,86,96]. Figure 3 also demonstrates that the silicon nanosphere generates an optical chirality flux an order of magnitude larger than the gold nanosphere of the same size.

Beyond the simple case of spherical nanoparticles shown in Figure 3, we now discuss distinct mechanisms which can contribute to enhancement of the optical chirality flux generated by metallic and dielectric nanostructures. The delocalized surface-electron gas, oscillating on resonance in metallic nanostructures [97], results in polarization and conduction currents which can interact in a sensitive and selective manner with chiral electromagnetic fields [61]. Thus, metallic nanoparticles exhibiting a left- or right-handed chiral geometry can effectively dissipate optical chirality and generate an optical

chirality flux [66,83,86,96]. A myriad of research efforts have, therefore, realized metallic nanostructures with complex chiral geometries, such as metallic helices, pyramids, dimers, and oligomers [10–28] (see also review articles [25,39–41]).

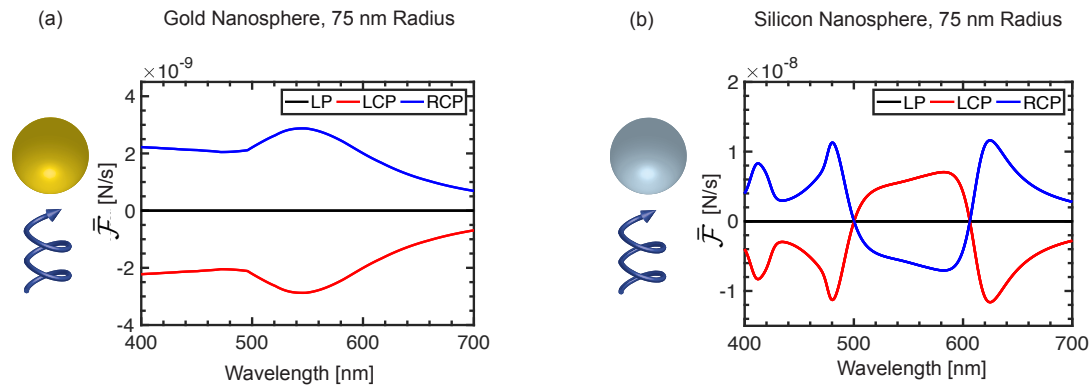


**Figure 3.** (a) Schematic illustration of a gold nanoparticle (spherical geometry, 75 nm radius) interacting with a circularly polarized plane wave. Numerical simulations of the total, volume-integrated optical chirality flux  $\bar{\mathcal{F}} = \int_V \nabla \cdot \mathcal{F} d^3x$  of the gold nanosphere upon excitation with linearly polarized (LP, black), left-handed circularly polarized light (CPL) (LCP, red), and right-handed CPL (RCP, blue). (b) Schematic illustration of a silicon nanoparticle (spherical geometry, 75 nm radius) interacting with a circularly polarized plane wave. Numerical simulations of the total, volume-integrated optical chirality flux  $\bar{\mathcal{F}}$  of the silicon nanosphere upon excitation with linearly polarized (LP, black), left-handed CPL (LCP, red), and right-handed CPL (RCP, blue).

In dielectric nanostructures, the conduction and polarization currents are considerably smaller than in metals [98]. Further, in the absence of primary sources, an intrinsic magnetic dipole moment arises from the magnetization current. Thus, tailoring the magnitude and phase shift of the intrinsic electric and magnetic dipole moments can enhance the chiral electromagnetic fields generated by dielectric nanostructures. This can be controlled by phase-shifted electric and magnetic fields in the excitation source, as is the case for CPL (Figure 3b), or further geometric tuning, as was demonstrated in recent research for achiral silicon nanospheres [29,30], silicon disk and sphere metasurfaces [32,33,35,36], or dielectric dimer structures [31,34,37,38]. These additional degrees of freedom inherent to the mechanism of chiral light–matter interactions in dielectric nanostructures enable the generation of highly enhanced chiral electromagnetic fields in simplified geometric configurations, suitable for high-throughput applications where strong optical chirality enhancement can be rationally designed in the nanostructure near field.

## 6. Conclusions

In conclusion, this perspective provides insight on the physical applicability of the optical helicity and the optical chirality in free space and in the presence of matter. In free space, a qualitative parallel between momentum in classical mechanics and optical helicity in classical electrodynamics can be made; likewise, a parallel between force and optical chirality also exists. We applied time and parity symmetry relations to demonstrate how the optical chirality density and flux quantify the handedness of an electromagnetic field. When chiral light interacts with macroscopic matter, we then identified how the optical helicity provides useful physical information for the case of lossless, dual-symmetric media, while the optical chirality provides physically observable information in the case of lossy, dispersive media. Here, a comparison to energy and momentum conservation for the lossless, elastic collision and the lossy, inelastic collision of two moving objects provides insight on the applicability of optical helicity and optical chirality conservation in the presence of matter. Finally, we applied the conservation law of optical chirality to numerically simulate the optical chirality flux generated

by a gold and silicon nanosphere of 75 nm radius. While no optical chirality flux was generated upon linearly polarized excitation, left- and right-handed CPL resulted in mirror-symmetric optical chirality flux spectra in both cases. This effect can be further enhanced by tuning the geometry of the nanostructure; while metallic nanostructures with a chiral shape direct the currents arising from the surface-electron gas, the interplay between electric and magnetic dipole moments in dielectric nanostructures affects the generation of chiral light. This information provides a platform from which researchers can improve the rational design of nanophotonic structures for the optimized enhancement of chiral light–matter interactions.

**Author Contributions:** Conceptualization, L.V.P., J.A.D. and A.G.-E.; methodology, L.V.P., J.A.D. and A.G.-E.; software, L.V.P.; validation, L.V.P., J.A.D. and A.G.-E.; formal analysis, L.V.P. and A.G.-E.; investigation, L.V.P., J.A.D. and A.G.-E.; resources, L.V.P., J.A.D. and A.G.-E.; data curation, L.V.P.; writing—original draft preparation, L.V.P.; writing—review and editing, L.V.P., J.A.D. and A.G.-E.; visualization, L.V.P.; supervision, J.A.D. and A.G.-E.; project administration, J.A.D. and A.G.-E.; funding acquisition, L.V.P., J.A.D. and A.G.-E.

**Funding:** This research was supported by the Swiss National Science Foundation Early Postdoc.Mobility Fellowship, project number P2EZIP2\_181595, Eusko Jaurlaritz, grant numbers PI-2016-1-0041, KK-2017/00089, IT1164-19 and KK-2019/00101, Ministerio de Economía, Industria y Competitividad, Gobierno de España grant number FIS2016-80174-P. A.G.-E. was funded by the Fellows Gipuzkoa fellowship of the Gipuzkoako Foru Aldundia through FEDER “Una Manera de hacer Europa”.

**Acknowledgments:** The authors thank David J. Norris, Lukas Novotny, Christian Hafner, Mark Lawrence, John Abendroth, Michelle Solomon, Jack Hu, David R. Barton III, Elissa Klopfer and Shing-Shing Ho for helpful scientific feedback. We thank Shing-Shing Ho for contributions to artistic rendering.

**Conflicts of Interest:** The authors declare no conflict of interest.

## References

1. Richardson, G. *The Foundations of Stereo Chemistry: Memoirs by Pasteur, Van't Hoff, Lebel and Wislicenus*; American Book Company: New York, NY, USA, 1901.
2. Eriksson, T.; Björkman, S.; Höglund, P. Clinical pharmacology of thalidomide. *Eu. J. Clin. Pharmacol.* **2001**, *57*, 365–376. [[CrossRef](#)] [[PubMed](#)]
3. Seo, J.S.; Whang, D.; Lee, H.; Im Jun, S.; Oh, J.; Jeon, Y.J.; Kim, K. A homochiral metal-organic porous material for enantioselective separation and catalysis. *Nature* **2000**, *404*, 982. [[CrossRef](#)] [[PubMed](#)]
4. Ma, L.; Abney, C.; Lin, W. Enantioselective catalysis with homochiral metal-organic frameworks. *Chem. Soc. Rev.* **2009**, *38*, 1248–1256. [[CrossRef](#)] [[PubMed](#)]
5. Blaser, H.U.; Federsel, H.J. *Asymmetric Catalysis on Industrial Scale: Challenges, Approaches and Solutions*; Wiley-VCH Verlag GmbH & Co. KGaA: Weinheim, Germany, 2004.
6. Tang, Y.; Cohen, A.E. Enhanced enantioselectivity in excitation of chiral molecules by superchiral light. *Science* **2011**, *332*, 333–336. [[CrossRef](#)] [[PubMed](#)]
7. Zhao, Y.; Saleh, A.A.; van de Haar, M.A.; Baum, B.; Briggs, J.A.; Lay, A.; Reyes-Becerra, O.A.; Dionne, J.A. Nanoscopic control and quantification of enantioselective optical forces. *Nat. Nanotechnol.* **2017**, *12*, 1055. [[CrossRef](#)] [[PubMed](#)]
8. Petersen, J.; Volz, J.; Rauschenbeutel, A. Chiral nanophotonic waveguide interface based on spin-orbit interaction of light. *Science* **2014**, *346*, 67–71. [[CrossRef](#)]
9. Le Feber, B.; Rotenberg, N.; Kuipers, L. Nanophotonic control of circular dipole emission. *Nat. Commun.* **2015**, *6*, 6695. [[CrossRef](#)]
10. Papakostas, A.; Potts, A.; Bagnall, D.; Prosvirnin, S.; Coles, H.; Zheludev, N. Optical manifestations of planar chirality. *Phys. Rev. Lett.* **2003**, *90*, 107404. [[CrossRef](#)]
11. Gansel, J.K.; Thiel, M.; Rill, M.S.; Decker, M.; Bade, K.; Saile, V.; von Freymann, G.; Linden, S.; Wegener, M. Gold helix photonic metamaterial as broadband circular polarizer. *Science* **2009**, *325*, 1513–1515. [[CrossRef](#)]
12. Hendry, E.; Carpy, T.; Johnston, J.; Popland, M.; Mikhaylovskiy, R.; Lapthorn, A.; Kelly, S.; Barron, L.; Gadegaard, N.; Kadodwala, M. Ultrasensitive detection and characterization of biomolecules using superchiral fields. *Nat. Nanotechnol.* **2010**, *5*, 783–787. [[CrossRef](#)]
13. Hentschel, M.; Schäferling, M.; Weiss, T.; Liu, N.; Giessen, H. Three-dimensional chiral plasmonic oligomers. *Nano Lett.* **2012**, *12*, 2542–2547. [[CrossRef](#)] [[PubMed](#)]

14. Zhao, Y.; Belkin, M.; Alù, A. Twisted optical metamaterials for planarized ultrathin broadband circular polarizers. *Nat. Commun.* **2012**, *3*, 870. [[CrossRef](#)] [[PubMed](#)]
15. Yin, X.; Schäferling, M.; Metzger, B.; Giessen, H. Interpreting chiral nanophotonic spectra: The plasmonic Born-Kuhn model. *Nano Lett.* **2013**, *13*, 6238–6243. [[CrossRef](#)] [[PubMed](#)]
16. Mark, A.G.; Gibbs, J.G.; Lee, T.C.; Fischer, P. Hybrid nanocolloids with programmed three-dimensional shape and material composition. *Nat. Mater.* **2013**, *12*, 802. [[CrossRef](#)] [[PubMed](#)]
17. Schamel, D.; Pfeifer, M.; Gibbs, J.G.; Miksch, B.R.; Mark, A.G.; Fischer, P. Chiral Colloidal Molecules and Observation of the Propeller Effect. *J. Am. Chem. Soc.* **2013**, *135*, 12353–12359. [[CrossRef](#)] [[PubMed](#)]
18. Schäferling, M.; Yin, X.; Engheta, N.; Giessen, H. Helical plasmonic nanostructures as prototypical chiral near-field sources. *ACS Photonics* **2014**, *1*, 530–537. [[CrossRef](#)]
19. McPeak, K.M.; van Engers, C.D.; Blome, M.; Park, J.H.; Burger, S.; Gosalvez, M.A.; Faridi, A.; Ries, Y.R.; Sahu, A.; Norris, D.J. Complex Chiral Colloids and Surfaces via High-Index Off-Cut Silicon. *Nano Lett.* **2014**, *14*, 2934–2940. [[CrossRef](#)]
20. Yeom, J.; Yeom, B.; Chan, H.; Smith, K.W.; Dominguez-Medina, S.; Bahng, J.H.; Zhao, G.; Chang, W.S.; Chang, S.J.; Chuvilin, A.; et al. Chiral templating of self-assembling nanostructures by circularly polarized light. *Nat. Mater.* **2015**, *14*, 66. [[CrossRef](#)]
21. Wang, L.Y.; Smith, K.W.; Dominguez-Medina, S.; Moody, N.; Olson, J.M.; Zhang, H.; Chang, W.S.; Kotov, N.; Link, S. Circular Differential Scattering of Single Chiral Self-Assembled Gold Nanorod Dimers. *ACS Photonics* **2015**, *2*, 1602–1610. [[CrossRef](#)]
22. McPeak, K.M.; van Engers, C.D.; Bianchi, S.; Rossinelli, A.; Poulikakos, L.V.; Bernard, L.; Herrmann, S.; Kim, D.K.; Burger, S.; Blome, M.; et al. Ultraviolet plasmonic chirality from colloidal aluminum nanoparticles exhibiting charge-selective protein detection. *Adv. Mater.* **2015**, *27*, 6244–6250. [[CrossRef](#)]
23. Tullius, R.; Karimullah, A.S.; Rodier, M.; Fitzpatrick, B.; Gadegaard, N.; Barron, L.D.; Rotello, V.M.; Cooke, G.; Laphorn, A.; Kadodwala, M. “Superchiral” spectroscopy: Detection of protein higher order hierarchical structure with chiral plasmonic nanostructures. *J. Am. Chem. Soc.* **2015**, *137*, 8380–8383. [[CrossRef](#)] [[PubMed](#)]
24. Koster, D.; De Hoogh, A.; Zeijlemaker, H.; Acar, H.; Rotenberg, N.; Kuipers, L. Core-shell plasmonic nanohelices. *ACS Photonics* **2017**, *4*, 1858–1863. [[CrossRef](#)] [[PubMed](#)]
25. Hentschel, M.; Schäferling, M.; Duan, X.; Giessen, H.; Liu, N. Chiral plasmonics. *Sci. Adv.* **2017**, *3*, e1602735. [[CrossRef](#)] [[PubMed](#)]
26. Karst, J.; Strohfeldt, N.; Schäferling, M.; Giessen, H.; Hentschel, M. Single plasmonic oligomer chiral spectroscopy. *Adv. Opt. Mater.* **2018**, *6*, 1800087. [[CrossRef](#)]
27. Lee, H.E.; Ahn, H.Y.; Mun, J.; Lee, Y.Y.; Kim, M.; Cho, N.H.; Chang, K.; Kim, W.S.; Rho, J.; Nam, K.T. Amino-acid-and peptide-directed synthesis of chiral plasmonic gold nanoparticles. *Nature* **2018**, *556*, 360. [[CrossRef](#)] [[PubMed](#)]
28. Karst, J.; Cho, N.H.; Kim, H.; Lee, H.E.; Nam, K.T.; Giessen, H.; Hentschel, M. Chiral scatterometry on chemically synthesized single plasmonic nanoparticles. *ACS Nano* **2019**. [[CrossRef](#)] [[PubMed](#)]
29. García-Etxarri, A.; Dionne, J.A. Surface-enhanced circular dichroism spectroscopy mediated by nonchiral nanoantennas. *Phys. Rev. B* **2013**, *87*, 235409. [[CrossRef](#)]
30. Ho, C.S.; Garcia-Etxarri, A.; Zhao, Y.; Dionne, J. Enhancing enantioselective absorption using dielectric nanospheres. *ACS Photonics* **2017**, *4*, 197–203. [[CrossRef](#)]
31. Zhang, W.; Wu, T.; Wang, R.; Zhang, X. Amplification of the molecular chiroptical effect by low-loss dielectric nanoantennas. *Nanoscale* **2017**, *9*, 5701–5707. [[CrossRef](#)] [[PubMed](#)]
32. Mohammadi, E.; Tsakmakidis, K.L.; Askarpour, A.N.; Dehkoda, P.; Tavakoli, A.; Altug, H. Nanophotonic platforms for enhanced chiral sensing. *ACS Photonics* **2018**, *5*, 2669–2675. [[CrossRef](#)]
33. Solomon, M.L.; Hu, J.; Lawrence, M.; García-Etxarri, A.; Dionne, J.A. Enantiospecific optical enhancement of chiral sensing and separation with dielectric metasurfaces. *ACS Photonics* **2018**, *6*, 43–49. [[CrossRef](#)]
34. Yao, K.; Liu, Y. Enhancing circular dichroism by chiral hotspots in silicon nanocube dimers. *Nanoscale* **2018**, *10*, 8779–8786. [[CrossRef](#)] [[PubMed](#)]
35. Graf, F.; Feis, J.; Garcia-Santiago, X.; Wegener, M.; Rockstuhl, C.; Fernandez-Corbaton, I. Achiral, helicity preserving, and resonant structures for enhanced sensing of chiral molecules. *ACS Photonics* **2019**, *6*, 482–491. [[CrossRef](#)]
36. Hanifeh, M.; Capolino, F. Helicity density enhancement in a planar array of achiral high-density dielectric nanoparticles. *arXiv* **2019**, arXiv:1905.03387.

37. Zhao, X.; Reinhard, B.M. Switchable Chiroptical Hot-Spots in Silicon Nanodisk Dimers. *ACS Photonics* **2019**. [[CrossRef](#)]
38. Mohammadi, E.; Tavakoli, A.; Dehkhoda, P.; Jahani, Y.; Tsakmakidis, K.L.; Tittl, A.; Altug, H. Accessible superchiral near-fields driven by tailored electric and magnetic resonances in all-dielectric nanostructures. *ACS Photonics* **2019**. [[CrossRef](#)]
39. Govorov, A.O.; Gun'ko, Y.K.; Slocik, J.M.; Gérard, V.A.; Fan, Z.; Naik, R.R. Chiral nanoparticle assemblies: Circular dichroism, plasmonic interactions, and exciton effects. *J. Mater. Chem.* **2011**, *21*, 16806–16818. [[CrossRef](#)]
40. Valev, V.K.; Baumberg, J.J.; Sibilica, C.; Verbiest, T. Chirality and chiroptical effects in plasmonic nanostructures: fundamentals, recent progress, and outlook. *Adv. Mater.* **2013**, *25*, 2517–2534. [[CrossRef](#)]
41. Ben-Moshe, A.; Maoz, B.M.; Govorov, A.O.; Markovich, G. Chirality and chiroptical effects in inorganic nanocrystal systems with plasmon and exciton resonances. *Chem. Soc. Rev.* **2013**, *42*, 7028–7041. [[CrossRef](#)]
42. Smith, K.W.; Link, S.; Chang, W.S. Optical characterization of chiral plasmonic nanostructures. *J. Photochem. Photobiol. C Photochem. Rev.* **2017**, *32*, 40–57. [[CrossRef](#)]
43. Barnett, S.M.; Cameron, R.P.; Yao, A.M. Duplex symmetry and its relation to the conservation of optical helicity. *Phys. Rev. A* **2012**, *86*, 013845. [[CrossRef](#)]
44. Crimin, F.; Mackinnon, N.; Götze, J.; Barnett, S. Optical helicity and chirality: Conservation and sources. *Appl. Sci.* **2019**, *9*, 828. [[CrossRef](#)]
45. Tung, W.K. *Group Theory in Physics: An Introduction to Symmetry Principles, Group Representations, and Special Functions in Classical and Quantum Physics*; World Scientific Publishing Company: Singapore, 1985.
46. Schwartz, M.D. *Quantum Field Theory and the Standard Model*; Cambridge University Press: Cambridge, UK, 2014.
47. Moffatt, H.K. The degree of knottedness of tangled vortex lines. *J. Fluid Mech.* **1969**, *35*, 117–129. [[CrossRef](#)]
48. Berger, M.A. Introduction to magnetic helicity. *Plasma Phys. Control. Fusion* **1999**, *41*, B167. [[CrossRef](#)]
49. Cameron, R.P. On the “second potential” in electrodynamics. *J. Opt.* **2013**, *16*, 015708. [[CrossRef](#)]
50. Fernandez-Corbaton, I.; Zambrana-Puyalto, X.; Tischler, N.; Vidal, X.; Juan, M.L.; Molina-Terriza, G. Electromagnetic duality symmetry and helicity conservation for the macroscopic maxwells equations. *Phys. Rev. Lett.* **2013**, *111*, 060401. [[CrossRef](#)] [[PubMed](#)]
51. Cameron, R.P.; Barnett, S.M.; Yao, A.M. Optical helicity, optical spin and related quantities in electromagnetic theory. *New J. Phys.* **2012**, *14*, 053050. [[CrossRef](#)]
52. Candlin, D. Analysis of the New Conservation Law in Electromagnetic Theory. *Il Nuovo Cimento (1955–1965)* **1965**, *37*, 1390–1395. [[CrossRef](#)]
53. Kibble, T. Conservation laws for free fields. *J. Math. Phys.* **1965**, *6*, 1022–1026. [[CrossRef](#)]
54. Tang, Y.; Cohen, A.E. Optical chirality and its interaction with matter. *Phys. Rev. Lett.* **2010**, *104*, 163901. [[CrossRef](#)]
55. Lipkin, D.M. Existence of a New Conservation Law in Electromagnetic Theory. *J. Math. Phys.* **1964**, *5*, 696–700. [[CrossRef](#)]
56. Noether, E. Invariante variations probleme. *Nachrichten von der Königlichen Gesellschaft der Wissenschaften zu Göttingen (Royal Society of Sciences, Göttingen)* **1918**, 235–257, 1918.
57. Calkin, M.G. An Invariance Property of the Free Electromagnetic Field. *Am. J. Phys.* **1965**, *33*, 958–960. [[CrossRef](#)]
58. Bliokh, K.Y.; Bekshaev, A.Y.; Nori, F. Dual electromagnetism: Helicity, spin, momentum and angular momentum. *New J. Phys.* **2013**, *15*, 033026. [[CrossRef](#)]
59. Sayir, M.; Dual, J.; Kaufmann, S. *Ingenieurmechanik 1*; Springer: Wiesbaden, Germany, 2008.
60. Hafner, C. (ETH Zürich, Zürich, ZH, Switzerland). Personal Communication, 2016.
61. Poulidakos, L.V. Chiral Light–Matter Interactions in the Near and Far Field. Ph.D. Thesis, ETH Zürich, Zürich, Switzerland, 2018.
62. Guasti, M.F. Chirality, helicity and the rotational content of electromagnetic fields. *Phys. Lett. A* **2019**, *383*, 3180–3186. [[CrossRef](#)]
63. Barron, L. *Chirality at the Nanoscale*; Wiley-VCH Verlag: Weinheim, BW, Germany; GmbH and Co. KGaA: Dusseldorf, Germany, 2009.
64. Jackson, J.D. *Classical Electrodynamics*, 3rd ed.; John Wiley & Sons, Inc.: New York, NY, USA, 1999.

65. Hafner, C. *Numerische Berechnung Elektromagnetischer Felder, Grundlagen, Methoden, Anwendungen*; Springer: Berlin/Heidelberg, Germany, 1987.
66. Poulidakos, L.V.; Gutsche, P.; McPeak, K.M.; Burger, S.; Niegemann, J.; Hafner, C.; Norris, D.J. Optical chirality flux as a useful far-field probe of chiral near fields. *ACS Photonics* **2016**, *3*, 1619–1625. [[CrossRef](#)]
67. Vázquez-Lozano, J.E.; Martínez, A. Optical chirality in dispersive and lossy media. *Phys. Rev. Lett.* **2018**, *121*, 043901. [[CrossRef](#)]
68. Philbin, T.G. Lipkin's conservation law, noether's theorem, and the relation to optical helicity. *Phys. Rev. A* **2013**, *87*, 043843. [[CrossRef](#)]
69. Van Kruining, K.; Götte, J.B. The conditions for the preservation of duality symmetry in a linear medium. *J. Opt.* **2016**, *18*, 085601. [[CrossRef](#)]
70. Nienhuis, G. Conservation laws and symmetry transformations of the electromagnetic field with sources. *Phys. Rev. A* **2016**, *93*, 023840. [[CrossRef](#)]
71. Alpeggiani, F.; Bliokh, K.; Nori, F.; Kuipers, L. Electromagnetic helicity in complex media. *Phys. Rev. Lett.* **2018**, *120*, 243605. [[CrossRef](#)] [[PubMed](#)]
72. Zambrana-Puyalto, X.; Vidal, X.; Juan, M.L.; Molina-Terriza, G. Dual and anti-dual modes in dielectric spheres. *Opt. Express* **2013**, *21*, 17520–17530. [[CrossRef](#)] [[PubMed](#)]
73. Zambrana-Puyalto, X.; Fernandez-Corbaton, I.; Juan, M.; Vidal, X.; Molina-Terriza, G. Duality symmetry and Kerker conditions. *Opt. Lett.* **2013**, *38*, 1857–1859. [[CrossRef](#)] [[PubMed](#)]
74. Schmidt, M.K.; Aizpurua, J.; Zambrana-Puyalto, X.; Vidal, X.; Molina-Terriza, G.; Sáenz, J.J. Isotropically polarized speckle patterns. *Phys. Rev. Lett.* **2015**, *114*, 113902. [[CrossRef](#)] [[PubMed](#)]
75. Allen, L.; Beijersbergen, M.W.; Spreeuw, R.; Woerdman, J. Orbital angular momentum of light and the transformation of Laguerre-Gaussian laser modes. *Phys. Rev. A* **1992**, *45*, 8185. [[CrossRef](#)] [[PubMed](#)]
76. Simpson, N.; Dholakia, K.; Allen, L.; Padgett, M. Mechanical equivalence of spin and orbital angular momentum of light: An optical spanner. *Opt. Lett.* **1997**, *22*, 52–54. [[CrossRef](#)]
77. Padgett, M.; Courtial, J.; Allen, L. Light's orbital angular momentum. *Phys. Today* **2004**, *57*, 35–40. [[CrossRef](#)]
78. García-Etxarri, A. Optical polarization mobius strips on all-dielectric optical scatterers. *ACS Photonics* **2017**, *4*, 1159–1164. [[CrossRef](#)]
79. Olmos-Trigo, J.; Sanz-Fernández, C.; García-Etxarri, A.; Molina-Terriza, G.; Bergeret, F.S.; Sáenz, J.J. Enhanced spin-orbit optical mirages from dual nanospheres. *Phys. Rev. A* **2019**, *99*, 013852. [[CrossRef](#)]
80. Olmos-Trigo, J.; Sanz-Fernández, C.; Abujetas, D.R.; García-Etxarri, A.; Molina-Terriza, G.; Sánchez-Gil, J.; Bergeret, S.F.; Sáenz, J.J. Role of the absorption on the spin-orbit interactions of light with Si nano-particles. *arXiv* **2019**, arXiv:1903.03816.
81. Fernandez-Corbaton, I.; Zambrana-Puyalto, X.; Molina-Terriza, G. Helicity and angular momentum: A symmetry-based framework for the study of light-matter interactions. *Phys. Rev. A* **2012**, *86*, 042103. [[CrossRef](#)]
82. Nieto-Vesperinas, M. Optical theorem for the conservation of electromagnetic helicity: Significance for molecular energy transfer and enantiomeric discrimination by circular dichroism. *Phys. Rev. A* **2015**, *92*, 023813. [[CrossRef](#)]
83. Poulidakos, L.V.; Thureja, P.; Stollmann, A.; De Leo, E.; Norris, D.J. Chiral light design and detection inspired by optical antenna theory. *Nano Lett.* **2018**, *18*, 4633–4640. [[CrossRef](#)] [[PubMed](#)]
84. Gutsche, P.; Poulidakos, L.V.; Hammerschmidt, M.; Burger, S.; Schmidt, F. Time-harmonic optical chirality in inhomogeneous space. In *Opto, Photonic and Phononic Properties of Engineered Nanostructures VI*; International Society for Optics and Photonics: San Francisco, CA, USA, 2016; Volume 9756, p. 97560X.
85. Collett, E. *Field Guide to Polarization*; SPIE Press: Bellingham, WA, USA, 2005; Volume FG05.
86. Schnoering, G.; Poulidakos, L.V.; Rosales-Cabara, Y.; Canaguier-Durand, A.; Norris, D.J.; Genet, C. Three-dimensional enantiomeric recognition of optically trapped single chiral nanoparticles. *Phys. Rev. Lett.* **2018**, *121*, 023902. [[CrossRef](#)] [[PubMed](#)]
87. Schäferling, M.; Dregely, D.; Hentschel, M.; Giessen, H. Tailoring enhanced optical chirality: Design principles for chiral plasmonic nanostructures. *Phys. Rev. X* **2012**, *2*, 031010. [[CrossRef](#)]
88. Choi, J.S.; Cho, M. Limitations of a Superchiral Field. *Phys. Rev. A* **2012**, *86*, 063834. [[CrossRef](#)]
89. Canaguier-Durand, A.; Genet, C. Chiral near fields generated from plasmonic optical lattices. *Phys. Rev. A* **2014**, *90*, 023842. [[CrossRef](#)]

90. Hanifeh, M.; Albooyeh, M.; Capolino, F. Helicity maximization of structured light to empower nanoscale chiral matter interaction. *arXiv* **2018**, arXiv:1809.04119.
91. Hanifeh, M.; Albooyeh, M.; Capolino, F. Empowering Structured Light to Enhance Chirality Detection and Characterization at Nanoscale. In *Opto, Complex Light and Optical Forces XIII*; International Society for Optics and Photonics: San Francisco, CA, USA, 2019; ; Volume 10935, p. 1093504.
92. Novotny, L.; Hecht, B. *Principles of Nano-Optics*, 2nd ed.; Cambridge University Press: New York, NY, USA, 2012.
93. Moffatt, H.K. Helicity and Singular Structures in Fluid Dynamics. *Proc. Natl. Acad. Sci. USA* **2014**, *111*, 3663–3670. [[CrossRef](#)] [[PubMed](#)]
94. Johnson, P.B.; Christy, R.W. Optical Constants of the Noble Metals. *Phys. Rev. B* **1972**, *6*, 4370. [[CrossRef](#)]
95. Aspnes, D.E.; Studna, A.A. Dielectric functions and optical parameters of Si, Ge, GaP, GaAs, GaSb, InP, InAs, and InSb from 1.5 to 6.0 Ev. *Phys. Rev. B* **1983**, *27*, 985. [[CrossRef](#)]
96. Hashiyada, S.; Narushima, T.; Okamoto, H. Imaging chirality of optical fields near achiral metal nanostructures excited with linearly polarized light. *ACS Photonics* **2018**, *5*, 1486–1492. [[CrossRef](#)]
97. Maier, S.A. *Plasmonics: Fundamentals and Applications*; Springer Science & Business Media: New York, NY, USA, 2007.
98. Capolino, F. *Theory and Phenomena of Metamaterials*; CRC Press/Taylor & Francis: Boca Raton, FL, USA, 2009.



© 2019 by the authors. Licensee MDPI, Basel, Switzerland. This article is an open access article distributed under the terms and conditions of the Creative Commons Attribution (CC BY) license (<http://creativecommons.org/licenses/by/4.0/>).